JOURNAL OF COMPUTER SCIENCE AND INFORMATICS ENGINEERING
VOL. 05, NO. 3, JULY 2026: 424-435
Doi: https://doi.org/10.55537/cosie.v5i3.1833

e-ISSN 2827-8356
p-ISSN 2827-9999

Robustness of YOLOv11n Model to Lighting Variations: Rice Leaf Disease Detection Case Study

Rangga Putra Sopyan*[1], Albert Yakobus Chandra [2]
[1,2] Information Systems Study Program, Faculty of Information Technology, Mercu Buana University, Yogyakarta, 55218, Indonesia
[1]221210029@student.mercubuana-yogyakarta.ac.id, [2] albert.ch@mercubuana-yogya.ac.id.

Received: June 12, 2026 | Revised: July 22, 2026 | Accepted: July 31, 2026

Abstract

Rice leaf diseases significantly reduce crop productivity, making accurate and reliable automatic detection essential for precision agriculture. Although recent YOLO-based approaches have achieved high detection accuracy under controlled conditions, the robustness of YOLOv11n against diverse lighting conditions in rice leaf disease detection remains insufficiently investigated, particularly under real-world field environments. This study evaluates the robustness of YOLOv11n using synthetic photometric transformations (S0-S11) and real field lighting conditions (L1-L4). Model performance was assessed using Precision, Recall, F1-Score, and mAP@0.5. Under baseline conditions, YOLOv11n achieved a Precision of 0,955, Recall of 0,936, F1-Score of 0,945, and mAP@0.5 of 0,949. The model remained highly robust to mild overexposure, mild underexposure, and saturation variations, while severe underexposure, extreme overexposure, and exposure scaling caused moderate to substantial degradation. Partial shadow produced the most severe performance decline, reducing mAP@0.5 by 90,20%. Furthermore, all real-world lighting scenarios exhibited performance drops exceeding 87%, revealing a pronounced domain gap between synthetic simulations and field conditions. These findings demonstrate that global photometric transformations alone are insufficient to represent complex real-world illumination, providing practical evidence for developing more robust lighting-aware object detection models for agricultural applications and emphasizing the importance of realistic robustness evaluation.

Keywords: YOLOv11n, rice leaf disease, lighting robustness, object detection, photometric transformation

1. INTRODUCTION

Rice (*Oryza sativa* L.) is a strategic food commodity that sustains the food security of more than half of the world's population, particularly in the Asian region. In Indonesia, rice serves as the staple food for the majority of the population, making rice productivity a crucial factor in national food availability [1], [2]. Nevertheless, Indonesia continues to face structural challenges in meeting domestic rice demand, one of which stems from leaf disease outbreaks that can cause yield losses of up to 37% per year if not detected early [3].

Rice leaf diseases frequently present distinctive visual symptoms, such as discoloration, lesion spots, and even necrosis on the leaf surface. Commonly encountered disease types include *Blast, Brown Spot, Leaf Blight, Leaf Scald,* and *Narrow Brown Spot* [4]. The visual similarity among these diseases is one of the factors that increases the risk of misdiagnosis in conventional inspection methods, which rely heavily on individual experience. Therefore, a more systematic, objective, and technology-based approach is needed to support faster, more consistent, and more accurate disease detection [5].

The advancement of *Deep Learning*, particularly *Convolutional Neural Network (CNN)* architectures and *You Only Look Once (YOLO)*-based object detection frameworks, has opened substantial opportunities for automating visual recognition in the agricultural sector [6].

e-ISSN 2827-8356
p-ISSN 2827-9999

Numerous prior studies have implemented various YOLO model variants to detect and classify plant diseases with continuously improving accuracy. YOLOv5 was reported to achieve an mAP of 75,1% in chili leaf disease detection [7], YOLOv7 combined with data augmentation achieved an mAP@0.5 of 95% for coffee leaf disease [8], and YOLOv8 recorded an exceptionally high performance with an mAP50 of 0,990 in durian leaf disease detection [9].

Although these models demonstrate excellent performance under controlled dataset conditions, their robustness to dynamic real-world lighting variations has not yet been comprehensively explored. Variations in light intensity during image acquisition can affect image quality and the stability of features extracted by the model, potentially causing a significant decline in system performance when deployed directly in the field [10]. A bibliometric review by Frontiers in AI (2025) explicitly identifies lighting variation, leaf occlusion, and environmental noise as major challenges that lead to accuracy degradation when models are applied in real-world field settings, characterizing this as an open research gap within the domain of deep learning-based plant monitoring [11]. Furthermore, models that achieve high performance under synthetic validation do not always maintain equivalent performance under real-world conditions, owing to the optical complexity of field environments that cannot be adequately represented through a single global manipulation [12].

The most recent development within the YOLO ecosystem is marked by the release of YOLOv11 by Ultralytics in September 2024. Compared to previous generations, YOLOv11 introduces improvements in network architecture, computational efficiency, and the ability to detect small objects such as disease lesions on leaves, making it well-suited for *real-time* plant monitoring on devices with limited computational resources [13], [14]. Unlike prior robustness studies that typically evaluate object detectors under a single lighting-manipulation pathway either synthetic photometric augmentation or naturally varying field conditions in isolation the present study explicitly combines both pathways within a unified evaluation framework, applying a quantified drop-percentage robustness taxonomy to directly measure and compare the domain gap between synthetic and real-world illumination for the same trained model. Based on this potential, the present study selects the YOLOv11n *(nano)* variant as the model whose robustness against lighting variation will be analyzed in the context of rice leaf disease detection.

2. METHODS

2.1 Research Flow

This study follows a systematic workflow consisting of five main stages as shown in Figure 1, Dataset Collection, Data Preprocessing, YOLOv11n Model Training, Simulation and Testing of Synthetic Lighting Scenarios (S0-S11) conducted in parallel with Field Image Collection and Testing under Real-World Conditions (L1-L4), and finally, Evaluation Metrics and Robustness Measurement as the concluding stage prior to drawing conclusions.

JOURNAL OF COMPUTER SCIENCE AND INFORMATICS ENGINEERING
VOL. 05, NO. 3, JULY 2026: 424-435
Doi: https://doi.org/10.55537/cosie.v5i3.1833
e-ISSN 2827-8356
p-ISSN 2827-9999

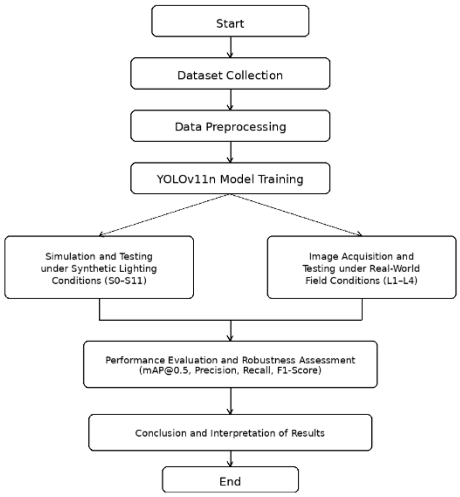

Figure 1. Research Stages

2.2 Dataset Collection

This study utilizes the Plant Detection Rice Leaf Disease dataset from the Roboflow platform [15], consisting of 1,551 rice leaf images across six classes Healthy, Brown Spot, Leaf Blast, Leaf Blight, Leaf Scald, and Narrow Brown Spot. The dataset was split at a 70:20:10 ratio for training, validation, and testing data, respectively. This proportion follows common practice in deep learning-based object detection research a study published in Statistical Analysis and Data Mining mathematically demonstrates that allocating a larger proportion of data to training relative to testing is an optimal practice for maximizing a model's ability to learn representative features prior to evaluation on an independent subset [16]. This split ensures that the model receives sufficiently representative training data while also maintaining independent validation and testing subsets for objectively measuring model generalization.

2.3 Data Preprocessing

All images were resized to 640×640 pixels to conform to the input dimensions required by the YOLOv11n architecture. Pixel values were normalized to the [0, 1] range to accelerate model convergence. Object annotations contained in .txt files were retained in YOLO format without modification, including class information and bounding box coordinates normalized relative to image dimensions.

2.4 YOLOv11n Model Training

This study employed the nano variant of the YOLOv11 architecture (YOLOv11n) due to its computational efficiency and suitability for real-time plant monitoring on resource-constrained devices [17]. The model was initialized using COCO pretrained weights as a foundation for transfer learning prior to fine-tuning on the rice leaf disease dataset. This approach has been shown to accelerate convergence, improve accuracy, and enhance generalization on agricultural datasets through the utilization of universal visual representations and the reduced need for large-scale domain-specific data annotation [18], [19], [20]. The complete training configuration is presented in Table 1.

Table 1. Training Hyperparameter Configuration

Parameter	Value
Epochs	100
Batch size	16
Input size	640 x 640
Optimizer	AdamW
Learning rate	0,001
Random Seed	42

JOURNAL OF COMPUTER SCIENCE AND INFORMATICS ENGINEERING
VOL. 05, NO. 3, JULY 2026: 424-435
Doi: https://doi.org/10.55537/cosie.v5i3.1833 e-ISSN 2827-8356
p-ISSN 2827-9999

Weight decay	0,0005
Training Augmentation	Flip, Mosaic
Pretrained Weights	COCO Dataset
Deterministic	True

Model training was performed using Ultralytics 8.4.37 with Python 3.12.13, PyTorch 2.10.0, and CUDA 12.8, on Google Colab leveraging an NVIDIA Tesla T4 GPU (15 GB VRAM). Robustness evaluation and inference were subsequently conducted using Ultralytics 8.4.60, Python 3.12.3, and PyTorch 2.12.0, running on an AMD Ryzen 5 5500U CPU to reflect a resource-constrained deployment scenario relevant to field applications.

2.5 Synthetic Lighting Scenario Simulation and Evaluation

Following the completion of the training process, the model's robustness was evaluated through simulated synthetic illumination variations on the testing set, implemented via Python-based photometric transformations using the OpenCV and NumPy libraries. The first primary method applied was Gamma Correction, implemented through a power-law transformation expressed by the following equation, where I_{out} denotes the output intensity, I_{in}^{γ}denotes the normalized input pixel value, and γ represents the gamma correction factor governing the image brightness level [21].

$$I_{out} = I_{in}^{\gamma}$$

This approach possesses strong physical justification as a mathematical representation of the non-linear response of camera sensors to light. Values of $\gamma < 1$ ($\gamma = 0{,}3$ and $\gamma = 0{,}6$) were used to simulate underexposure conditions, whereas values of $\gamma > 1$ ($\gamma = 1{,}5$ and $\gamma = 2{,}5$) were applied to simulate overexposure conditions [22].

The second method involved manipulation of the HSV color space to simulate variations in color saturation and partial shadowing [23]. The advantage of this method lies in its capacity to independently separate brightness (value) and saturation information without introducing cross-channel correlation [24]. In this study, the S channel was manipulated by ±40% to simulate Low Saturation (S8) and High Saturation (S9), while the V channel was subjected to a masking technique applied to 50% of the image area to simulate Partial Shadow (S5). The trained model was subsequently subjected directly to inference across all simulation scenarios without any retraining stage.

The third method consisted of linear additive brightness adjustment, in which a constant value β was added to or subtracted from the pixel intensity ($\beta = -40$ for S6 and $\beta = +40$ for S7) to uniformly shift the global intensity histogram without altering the relative ratio between pixels. This technique served as a controlled augmentation tool for enhancing model generalization without obscuring relevant objects [25], [26].

Finally, the fourth method applied multiplicative exposure scaling, expressed by the following equation, where I_{out} denotes the output intensity, I_{in} denotes the input pixel intensity, α represents the exposure scaling factor governing the global brightness level of the image, and γ represents the gamma correction factor controlling the non-linear transformation of pixel intensity.

$$I_{out} = \alpha \times I_{in}^{\gamma}$$

which is mathematically equivalent to scaling the physical light power illuminating the object. Unlike brightness adjustment, exposure-induced degradation is proportional to the original pixel value, with $\alpha = 0{,}7$ used to simulate Low Exposure (S10) and $\alpha = 1{,}3$ used to simulate High Exposure (S11). The complete details of all experimental scenarios are presented in Table 2.

JOURNAL OF COMPUTER SCIENCE AND INFORMATICS ENGINEERING
VOL. 05, NO. 3, JULY 2026: 424-435
Doi: https://doi.org/10.55537/cosie.v5i3.1833 e-ISSN 2827-8356
p-ISSN 2827-9999

Table 2. Synthetic Lighting Scenario Configuration

Code	Scenario	Method	Parameter
S0	Normal (Baseline)	Without transformation	-
S1	Mild Overexposure	Gamma correction	γ = 1,5
S2	Severe Overexposure	Gamma correction	γ = 2,5
S3	Mild Underexposure	Gamma correction	γ = 0,6
S4	Severe Underexposure	Gamma correction	γ = 0,3
S5	Partial Shade	Masking HSV-Value	50% dark area
S6	Low Brightness	Brightness reduction	β = -40
S7	High Brightness	Increased brightness	β = +40
S8	Low Saturation	S channel drop	-40%
S9	High Saturation	S channel enhancement	+40%
S10	Low Exposure	Intensity scaling	α = 0,7
S11	High Exposure	Intensity scaling	α = 1,3

2.6 Real-World Field Image Acquisition and Evaluation

In parallel with the synthetic pathway, rice leaf images were collected directly in the field under four distinct real-world lighting conditions. Images were captured at agricultural sites using a consistent Samsung A05s smartphone camera operated in a handheld manner without a tripod, with an acquisition distance of approximately 5-10 cm from the rice leaf surface. This image acquisition protocol was intentionally designed to simulate realistic, unconstrained image-capture scenarios similar to those performed by farmers using consumer-grade smartphone devices under actual field conditions, rather than relying on standardized laboratory imaging equipment. The same trained model was then used for inference on these field images without any retraining to evaluate its robustness under natural illumination variations. The four field conditions tested are presented in Table 3.

Table 3. Field Lighting Scenarios

Code	Condition	Description	Number of Images
L1	Morning	Low-medium lighting, cool color temperature, low light angle (± 07.00-08.00 WIB)	35 Images
L2	Afternoon	High lighting, minimal shadows, high contrast (± 11.00-13.00 WIB)	33 Images
L3	Evening	Low-medium lighting, warm color temperature, low light angle (± 15.00-17.00 WIB)	31 Images
L4	Plant Shade Area	Uneven local lighting due to the shade of the surrounding plant canopy	29 Images

JOURNAL OF COMPUTER SCIENCE AND INFORMATICS ENGINEERING
VOL. 05, NO. 3, JULY 2026: 424-435
Doi: https://doi.org/10.55537/cosie.v5i3.1833 e-ISSN 2827-8356
p-ISSN 2827-9999

2.7 Performance Evaluation and Robustness Assessment

All inference results from both the synthetic and field scenarios were evaluated in aggregate and on a per-class basis using four primary metrics: Precision, Recall, F1-Score, and mAP@0.5. The degree of performance degradation was calculated based on the difference in mAP@0.5 relative to the baseline (S_0) via the equation $\Delta mAP = mAP(S_0) - mAP(S_i/L_i)$, where a larger ΔmAPvalue indicates greater performance degradation resulting from illumination variation. This analysis aimed to identify degradation patterns, map the underlying visual failure mechanisms, and quantify the magnitude of the domain gap between synthetic and real-world field conditions. Robustness categories were then defined based on the percentage decline values as follows: Highly Robust ($\leq$ 5%), Robust (5-15%), Moderately Robust (15-30%), and Non-Robust (> 30%).

During inference, a confidence threshold of 0,498 and a Non-Maximum Suppression (NMS) IoU threshold of 0,70 were applied consistently across all validation, synthetic, and field evaluation scenarios. The confidence threshold was selected based on the maximum point of the F1-Confidence Curve obtained from the validation set Figure 2, corresponding to an overall F1-score of approximately 0,93. This inference configuration was fixed throughout all experiments to ensure an optimal balance between precision and recall while maintaining consistency and reproducibility across different illumination conditions.

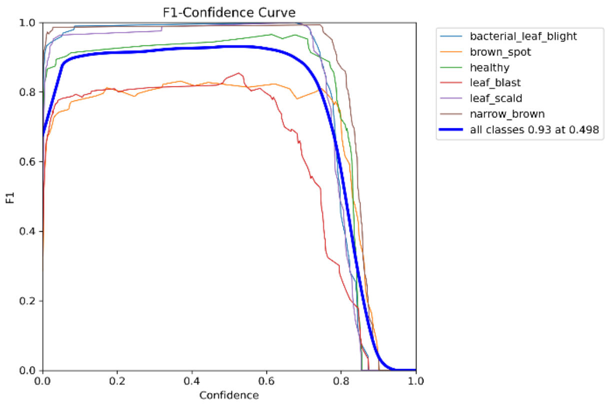

Figure 2. F1–Confidence Curve of the YOLOv11n model on the validation dataset.

3. RESULT AND DISCUSSION

This section presents the results and analysis of each stage of the research workflow sequentially, beginning with dataset distribution, preprocessing results, model training performance, the results of testing across eleven synthetic lighting scenarios, the results of testing under four real-world field conditions, and concluding with a comprehensive robustness measurement.

3.1 Dataset Preparation and Distribution

The dataset consists of 1,551 images, partitioned into training, validation, and testing subsets as detailed in Table 4. To ensure unbiased evaluation and to mitigate class imbalance effects, we employed a stratified sampling approach.

Table 4. Dataset Distribution

Subset	Proportion	Images
Training Set	70%	1,086
Validation Set	20%	310
Testing Set	10%	155
Total	100%	1,551

JOURNAL OF COMPUTER SCIENCE AND INFORMATICS ENGINEERING
VOL. 05, NO. 3, JULY 2026: 424-435
Doi: https://doi.org/10.55537/cosie.v5i3.1833 e-ISSN 2827-8356
p-ISSN 2827-9999

3.2 Preprocessing Result

All 1,551 images were successfully processed and converted to a resolution of 640×640 pixels, with no data dropped. Pixel normalization to the [0, 1] range was applied consistently across all three subsets. An annotation integrity check confirmed that all corresponding .txt files were present and contained valid bounding box coordinates for every image. No images lacking annotations were found, nor were any annotations found to exceed the image coordinate boundaries. These preprocessing results ensured that the input received by the model during training and testing maintained consistent quality and integrity.

3.3 YOLOv11n Model Training Results (Baseline)

The YOLOv11n model achieved stable convergence within 100 training epochs, exhibiting a minimal generalization gap between the training and validation trajectories across all loss components Figure 3.

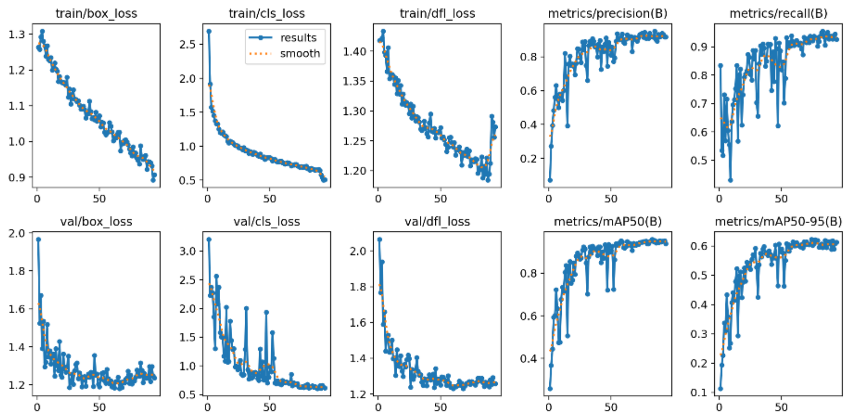

Figure 3. Training and validation loss curves.

As illustrated in Figure 3, the box loss exhibits a consistent decay across both data partitions, indicating the model's enhanced precision in spatial bounding box regression. The simultaneous decline in classification loss validates the network's capacity to extract highly discriminative features without signs of overfitting. Furthermore, the stabilization of the distribution focal loss (DFL) confirms that the predicted object location distributions have successfully converged. The absence of a significant generalization gap between the training and validation curves corroborates the attainment of optimal convergence. Using the inference configuration described in Section 2.7, the baseline model was evaluated on the independent testing set and achieved robust performance metrics: mAP@0.5 = 0,9491, Precision = 0,9553, Recall = 0,9355, and F1-Score = 0,9453.

Table 5. Class-wise Average Precision (AP@0.5)

Class	**AP@0.5**
Bacterial Leaf Blight	0,995
Leaf Scald	0,995
Narrow Brown Spot	0,994
Healthy	0,973
Leaf Blast	0,863
Brown Spot	0,856
Average	**0,946**

Doi: https://doi.org/10.55537/cosie.v5i3.1833
e-ISSN 2827-8356
p-ISSN 2827-9999

Table 5 presents the class-specific Average Precision (AP) under the baseline configuration. The Bacterial Leaf Blight, Leaf Scald, Narrow Brown Spot, and Healthy classes achieved AP scores exceeding 0,97, demonstrating the model's superior feature discrimination capabilities. Conversely, a noticeable performance degradation was observed in the Leaf Blast (AP = 0,863) and Brown Spot (AP = 0,856) classes. This lower accuracy is primarily driven by morphological ambiguities, specifically the high overlap in color signatures and lesion textures between these two manifestations, which confounds the model's classification boundary

3.4 Synthetic Lighting Variation Robustness Test Results

To evaluate the operational robustness of the trained model, stress testing was conducted across 12 distinct illumination scenarios (S0 to S11), leveraging the ideal lighting condition (S0) as the performance baseline The comprehensive performance metrics for all simulated scenarios are detailed in Table 6.

Table 6. Results of Model Robustness Tests to Lighting Variations

Code	Scenario	Precision	Recall	F1-Score	mAP@0.5	Drop (%)	Category
S0	Normal (Baseline)	0,955	0,936	0,945	0,949	0,00	-
S1	Mild Overexposure	0,944	0,920	0,932	0,934	1,55	Very Robust
S2	Severe Overexposure	0,845	0,615	0,712	0,757	20,24	Moderately Robust
S3	Mild Underexposure	0,948	0,894	0,920	0,924	2,61	Very Robust
S4	Severe Underexposure	0,778	0,597	0,676	0,661	30,38	Not Robust
S5	Partial Shade	0,116	0,166	0,137	0,093	90,20	Not Robust
S6	Low Brightness	0,925	0,811	0,864	0,872	8,18	Robust
S7	High Brightness	0,872	0,711	0,783	0,813	14,35	Robust
S8	Low Saturation	0,961	0,886	0,922	0,923	2,78	Very Robust
S9	High Saturation	0,950	0,936	0,943	0,949	0,04	Very Robust
S10	Low Exposure	0,925	0,612	0,737	0,776	18,29	Moderately Robust
S11	High Exposure	0,871	0,646	0,742	0,775	18,32	Moderately Robust

Under low-illumination variations, the model exhibited asymmetric robustness depending on manipulation intensity. S3 ($\gamma = 0,6$) was categorized as Very Robust, achieving mAP@0.5 = 0,924 (a 2,61% drop), as moderate dimming did not degrade morphological features, whereas S4 ($\gamma = 0,3$) was categorized as Non-Robust, with mAP@0.5 = 0,661 (30,38% drop), resulting from extreme non-linear gamma compression that eliminated color gradation and lesion texture details. In contrast, the degradation observed under S6 ($\beta = -40$) was more moderate (mAP@0.5 = 0,872, an 8.18% drop, Robust), as linear brightness reduction did not suppress dark pixel values as severely as gamma compression. Under high-illumination variations, S1 ($\gamma = 1,5$) demonstrated optimal robustness (a 1,55% drop, Very Robust), whereas S2 ($\gamma = 2,5$) triggered a decline in mAP@0.5 to 0,757 (a 20,24% drop, Moderately Robust) due to pixel saturation and bleaching effects, and S7 ($\beta = +40$) yielded mAP@0.5 = 0,813 (a 14.35% drop, Robust). Regarding saturation variations, YOLOv11n was shown to rely more heavily on textural and shape pattern features than on pure color intensity, as evidenced by S8 (-40%), which yielded mAP@0.5 = 0,923 (a 2,78% drop, Very Robust), and S9 (+40%), which was nearly identical to the baseline (a 0,04% drop, Very Robust). With respect to exposure scaling, S10 and S11

JOURNAL OF COMPUTER SCIENCE AND INFORMATICS ENGINEERING
VOL. 05, NO. 3, JULY 2026: 424-435
Doi: https://doi.org/10.55537/cosie.v5i3.1833 e-ISSN 2827-8356
p-ISSN 2827-9999

produced symmetric declines (drops of 18,29% and 18,32%, respectively, Moderately Robust), demonstrating an equivalent impact from both the reduction and amplification of uniform intensity. Finally, S5 (Partial Shadow) emerged as the most destructive scenario, with mAP@0.5 of only 0,093 (a 90,20% drop, Non-Robust).

3.5 Robustness to Real Field Conditions

Testing under four real-world field conditions (L1-L4) revealed a markedly significant domain gap relative to the synthetic scenarios. The complete results are presented in Table 7.

Table 7. Performance of YOLOv11n Model under Real Field Conditions

Code	**Condition**	**Precision**	**Recall**	**F1-Score**	**mAP@0.5**	**Drop (%)**	**Category**
L1	Morning (07.00-08.00)	0,115	0,144	0,128	0,121	87,25	Not Robust
L2	Afternoon (11.00-13.00)	0,304	0,181	0,227	0,117	87,69	Not Robust
L3	Evening (15.00-17.00)	0,082	0,167	0,110	0,101	89,39	Not Robust
L4	Plant Shade Area	0,579	0,095	0,164	0,083	91,21	Not Robust

The test results revealed a significant performance decline between the baseline condition (S_0: mAP@0.5 = 0,949; F1-Score = 0,945) and the real-world field conditions of morning (L_1: mAP@0.5 = 0,121) and midday (L_2: mAP@0.5 = 0,117), with degradation exceeding 87%. This decline indicates that a model trained without illumination variation tends to learn illumination-dependent features, thereby constraining its generalization capability due to domain gap and color domain shift arising from natural color temperature changes. In the morning, specular reflection from dew generated visual noise that obscured lesion texture details and increased false negatives, whereas at midday, high light intensity induced overexposure and a bleaching effect that reduced contrast, alongside sharp inter-leaf shadows that interfered with object localization. This performance disparity demonstrates that homogeneous synthetic transformations are unable to represent the complexity of real-world optical interactions, which involve the simultaneous combination of multiple visual degradation factors [11], [27]. These findings underscore that high performance under controlled conditions does not guarantee successful real-world deployment [12] without the integration of field data or adaptive photometric augmentation.

4. CONCLUSION

The YOLOv11n model demonstrated excellent detection performance under normal illumination conditions (mAP@0.5 = 0,949, F1-Score = 0,945) and exhibited varying degrees of robustness to synthetic illumination variations. The model was highly robust to changes in color saturation and mild overexposure, moderately robust to brightness and exposure variations, but non-robust to partial shadow and severe underexposure. Overall, illumination variation affected the recall metric more substantially than precision, and the pattern of performance decline was non-linear as the manipulation intensity increased.The most critical finding was the substantial domain gap between synthetic and real-world field conditions, in which all field scenarios exhibited a decline in mAP@0.5 exceeding 87%, far surpassing even the most severe synthetic scenario. This demonstrates that single, global photometric transformations are not yet capable of representing the complexity of real-world illumination, which involves the simultaneous interaction of multiple physical factors. It should be noted that the reported metrics represent single-run evaluations for each lighting scenario; statistical validation through repeated trials with

e-ISSN 2827-8356
p-ISSN 2827-9999

multiple random seeds and the computation of confidence intervals were beyond the scope of this study. To improve model robustness and statistical reliability, future research is encouraged to integrate more realistic illumination augmentation (spatial shadow augmentation, color temperature shift simulation), expand the training data with real-world field samples collected across various times and locations, explore adaptive preprocessing methods such as CLAHE or Retinex-based approaches to stabilize image intensity distribution prior to inference, and validate the observed robustness patterns through repeated experimental trials.

ACKNOWLEDGMENTS

The authors would like to thank Universitas Mercu Buana Yogyakarta for institutional support during this research

CONFLICT OF INTEREST

The authors declare that they have no known competing financial interests or personal relationships that could have appeared to influence the work reported in this paper.

REFERENCES

[1] P. Preethi, R. Swathika, S. Kaliraj, R. Premkumar, and J. Yogapriya, “Deep Learning–Based Enhanced Optimization for Automated Rice Plant Disease Detection and Classification,” *Food Energy Secur.*, vol. 13, no. 5, Sep. 2024, doi: 10.1002/fes3.70001.

[2] Afis Julianto, Andi Sunyoto, and Ferry Wahyu Wibowo, “Optimasi Hyperparameter Convolutional Neural Network Untuk Klasifikasi Penyakit Tanaman Padi,” *TEKNIMEDIA: Teknologi Informasi dan Multimedia*, vol. 3, no. 2, pp. 98–105, Dec. 2022, doi: 10.46764/teknimedia.v3i2.77.

[3] M. E. Rana, V. A. Hameed, I. K. Y. Eng, H. K. Tripathy, and S. Mallik, “Harnessing artificial intelligence for sustainable rice leaf disease classification,” *Front. Plant Sci.*, vol. 16, Sep. 2025, doi: 10.3389/fpls.2025.1594329.

[4] G. Latif, S. E. Abdelhamid, R. E. Mallouhy, J. Alghazo, and Z. A. Kazimi, “Deep Learning Utilization in Agriculture: Detection of Rice Plant Diseases Using an Improved CNN Model,” *Plants*, vol. 11, no. 17, p. 2230, Aug. 2022, doi: 10.3390/plants11172230.

[5] I. Ahmed and P. K. Yadav, “A systematic analysis of machine learning and deep learning based approaches for identifying and diagnosing plant diseases,” *Sustainable Operations and Computers*, vol. 4, pp. 96–104, 2023, doi: 10.1016/j.susoc.2023.03.001.

[6] C. Gupta *et al.*, “Deep vision in agriculture: assessing the function of YOLO in the classification of plant leaf diseases (PLDs),” *BioData Min.*, vol. 18, no. 1, p. 91, Nov. 2025, doi: 10.1186/s13040-025-00497-y.

[7] N. M. Yasen, S. Rifka, R. Vitria, and Y. Yulindon, “Pemanfaatan Yolo Untuk Deteksi Hama Dan Penyakit Pada Daun Cabai Menggunakan Metode Deep Learning,” *Elektron : Jurnal Ilmiah*, pp. 63–71, Dec. 2023, doi: 10.30630/eji.0.0.397.

[8] A. Ardiansyah and N. F. Hasan, “Deteksi dan Klasifikasi Penyakit Pada Daun Kopi Menggunakan Yolov7,” *Jurnal Sisfokom (Sistem Informasi dan Komputer)*, vol. 12, no. 1, pp. 30–35, Mar. 2023, doi: 10.32736/sisfokom.v12i1.1545.

e-ISSN 2827-8356
p-ISSN 2827-9999

[9] R. R. Putra, M. Maimunah, and D. Sasongko, “Implementasi Algoritma YOLO V8 (You Only Look Once) Dalam Deteksi Penyakit Daun Durian,” *Building of Informatics, Technology and Science (BITS)*, vol. 6, no. 3, Dec. 2024, doi: 10.47065/bits.v6i3.6136.

[10] W. Zhong *et al.*, “Light adaptive image enhancement for improving visual analysis in intercropping cultivation,” *Front. Plant Sci.*, vol. 16, Aug. 2025, doi: 10.3389/fpls.2025.1639016.

[11] R. Zhang *et al.*, “A bibliometric review of deep learning in crop monitoring: trends, challenges, and future perspectives,” *Front. Artif. Intell.*, vol. 8, Sep. 2025, doi: 10.3389/frai.2025.1636898.

[12] C. Zhang, X. Hao, J. Liang, L. Li, and W. Li, “A lightweight and generalizable deep learning framework for early detection of rice leaf diseases in complex field environments,” *Sci. Rep.*, vol. 15, no. 1, p. 45098, Dec. 2025, doi: 10.1038/s41598-025-32568-9.

[13] H. Teng, Y. Wang, W. Li, T. Chen, and Q. Liu, “Advancing Rice Disease Detection in Farmland with an Enhanced YOLOv11 Algorithm,” *Sensors*, vol. 25, no. 10, p. 3056, May 2025, doi: 10.3390/s25103056.

[14] L. T. Ramos and A. D. Sappa, “A comprehensive analysis of YOLO architectures for tomato leaf disease identification,” *Sci. Rep.*, vol. 15, no. 1, p. 26890, Jul. 2025, doi: 10.1038/s41598-025-11064-0.

[15] Tru Projects, 2023, "plantdet rice leaf disease setection Computer Vision Model" Roboflow Universe. [Online]. Available: https://universe.roboflow.com/tru-projects-cqcql/plantdet-rice-leaf-disease-setection.

[16] V. R. Joseph, “Optimal ratio for data splitting,” *Statistical Analysis and Data Mining: The ASA Data Science Journal*, vol. 15, no. 4, pp. 531–538, Aug. 2022, doi: 10.1002/sam.11583.

[17] A. Rana and P. Vaidya, “YOLO-based deep learning framework for real-time multi-class plant health monitoring in precision agriculture,” *Sci. Rep.*, vol. 16, no. 1, p. 197, Jan. 2026, doi: 10.1038/s41598-025-29132-w.

[18] M. H. Saleem, J. Potgieter, and K. M. Arif, “A weight optimization-based transfer learning approach for plant disease detection of New Zealand vegetables,” *Front. Plant Sci.*, vol. 13, Oct. 2022, doi: 10.3389/fpls.2022.1008079.

[19] Q. Fan, R. Chen, and B. Li, “Rice disease detection method based on multi-scale dynamic feature fusion,” *Front. Plant Sci.*, vol. 16, May 2025, doi: 10.3389/fpls.2025.1543986.

[20] C. K. Sunil, C. D. Jaidhar, and N. Patil, “Systematic study on deep learning-based plant disease detection or classification,” *Artif. Intell. Rev.*, vol. 56, no. 12, pp. 14955–15052, Dec. 2023, doi: 10.1007/s10462-023-10517-0.

[21] X. Li, M. Liu, and Q. Ling, “Pixel-Wise Gamma Correction Mapping for Low-Light Image Enhancement,” *IEEE Transactions on Circuits and Systems for Video Technology*, vol. 34, no. 2, pp. 681–694, Feb. 2024, doi: 10.1109/TCSVT.2023.3286802.

e-ISSN 2827-8356
p-ISSN 2827-9999

[22] S. Junzhe and Z. Zhibin, "Unsupervised low-light image enhancement by data augmentation and contrastive learning," *The Imaging Science Journal*, vol. 73, no. 3, pp. 354–362, Apr. 2025, doi: 10.1080/13682199.2024.2395751.

[23] S. U. A. Shovo, Md. G. R. Abir, Md. M. Kabir, and M. F. Mridha, "Advancing low-light object detection with you only look once models: An empirical study and performance evaluation," *Cognitive Computation and Systems*, vol. 6, no. 4, pp. 119–134, Dec. 2024, doi: 10.1049/ccs2.12114.

[24] I. Hussain and R. Ali, "Robust Leaf Disease Detection Using Complex Fuzzy Sets and HSV-Based Color Segmentation Techniques," *Acadlore Transactions on AI and Machine Learning*, vol. 3, no. 3, pp. 183–192, Sep. 2024, doi: 10.56578/ataiml030305.

[25] A. Y. Ashurov *et al.*, "Enhancing plant disease detection through deep learning: a Depthwise CNN with squeeze and excitation integration and residual skip connections," *Front. Plant Sci.*, vol. 15, Jan. 2025, doi: 10.3389/fpls.2024.1505857.

[26] K. Antwi, K. E. Bennin, D. K. Pobi Asiedu, and B. Tekinerdogan, "On the application of image augmentation for plant disease detection: A systematic literature review," *Smart Agricultural Technology*, vol. 9, p. 100590, Dec. 2024, doi: 10.1016/j.atech.2024.100590.

[27] S. Gholinavaz, N. saeedi, and S. S. Gharehveran, "Robustness analysis of YOLO and faster R-CNN for object detection in realistic weather scenarios with noise augmentation," *Sci. Rep.*, vol. 15, no. 1, p. 44888, Dec. 2025, doi: 10.1038/s41598-025-28737-5.